

Interaction effects on galaxy pairs with Gemini/GMOS- II: Oxygen abundance gradients

D. A. Rosa^{1*}, O. L. Dors Jr.¹, A. C. Krabbe¹, G. F. Hägele^{2,3}, M. V. Cardaci^{2,3},
M. G. Pastoriza⁴, I. Rodrigues¹, C. Winge⁵.

¹ *Universidade do Vale do Paraíba, Av. Shishima Hifumi, 2911, Cep 12244-000, São José dos Campos, SP, Brazil*

² *Instituto de Astrofísica de La Plata (CONICET La Plata–UNLP), Argentina.*

³ *Facultad de Ciencias Astronómicas y Geofísicas, Universidad Nacional de La Plata, Paseo del Bosque s/n, 1900 La Plata, Argentina*

⁴ *Instituto de Física, Universidade Federal do Rio Grande do Sul, Av. Bento Gonçalves, 9500, Cep 91359-050, Porto Alegre, RS, Brazil*

⁵ *Gemini Observatory, c/o AURA Inc., Casilla 603, La Serena, Chile*

Accepted -. Received -.

ABSTRACT

In this paper we derived oxygen abundance gradients from H II regions located in eleven galaxies in eight systems of close pairs. Long-slit spectra in the range 4400–7300 Å were obtained with the Gemini Multi-Object Spectrograph at Gemini South (GMOS). Spatial profiles of oxygen abundance in the gaseous phase along galaxy disks were obtained using calibrations based on strong emission-lines ($N2$ and $O3N2$). We found oxygen gradients significantly flatter for all the studied galaxies than those in typical isolated spiral galaxies. Four objects in our sample, AM 1219A, AM 1256B, AM 2030A and AM 2030B, show a clear break in the oxygen abundance at galactocentric radius R/R_{25} between 0.2 and 0.5. For AM 1219A and AM 1256B we found negative slopes for the inner gradients, and for AM 2030B we found a positive one. In all these three cases they show a flatter behaviour to the outskirts of the galaxies. For AM 2030A, we found a positive-slope outer gradient while the inner one is almost compatible with a flat behaviour. A decrease of star formation efficiency in the zone that corresponds to the oxygen abundance gradient break for AM 1219A and AM 2030B was found. For the former, a minimum in the estimated metallicities was found very close to the break zone that could

be associated with a corotation radius. On the other hand, AM 1256B and AM 2030A, present a SFR maximum but not an extreme oxygen abundance value. All the four interacting systems that show oxygen gradient breaks the extreme SFR values are located very close to break zones. H II regions located in close pairs of galaxies follow the same relation between the ionization parameter and the oxygen abundance as those regions in isolated galaxies.

Key words: interactions galaxy: spectroscopy galaxies abundances: ISM: abundances:

1 INTRODUCTION

The study of the chemical evolution of galaxies, both isolated and interacting, play an important role to understand the formation of these objects, its stellar formation history and the evolution of the Universe.

In general, for almost all disk isolated galaxies a negative oxygen gradient is derived, such as our Galaxy (Bragaglia et al. 2008; Magrini et al. 2009; Yong et al. 2014; Pedicelli et al. 2009; Andrievsky et al. 2002, 2004; Luck et al. 2003; Lemasle et al. 2013; Esteban et al. 2013; Vílchez et al. 1996; Costa et al. 2004; Maciel & Costa 2009). This negative gradient is naturally explained by models which assume the growth in the inside-out scenario of galaxies (Portinari & Chiosi 1999; Boissier & Prantzos 2000; Móra & Díaz 2005), where galaxies begin to form their inner regions before the outer ones, as confirmed by stellar populations studies of spiral galaxies (Bell & Jong 2000; MacArthur et al. 2004; Pohlen & Trujillo 2006; Muñoz-Mateos et al. 2007) and by very deep photometric studies of galaxies at high redshifts (Trujillo et al. 2004; Barden et al. 2005).

The oxygen gradients can be flattened or modified by the presence of gas flows along the galactic disk. Basically, these gas flows could be arise due to two mechanisms. In isolated galaxies, hydro-dynamical simulations predict that the bars may produce a falling of gas into the central regions (Athanasoula 1992; Friedli et al. 1994) which have been confirmed by observational studies (Zaritsky et al. 1994; Martin & Roy 1994). The second mechanism occur in interacting galaxies or close pairs, where interaction-induced gas flows from the outer parts to the centre of each component (Dalcanton 2007; Toomre & Toomre 1972) seem to modify the metallicity in galactic disks. Therefore, the metallicity gradients of interacting

galaxies or galaxies that have had an interaction in the past are shallower (Sánchez et al. 2014; Miralles-Caballero et al. 2014; Rupke et al. 2010a; Bresolin et al. 2009) than the ones derived for isolated galaxies (Sánchez et al. 2012; Rupke et al. 2010a). In fact, Krabbe et al. (2008, 2011) combining long-slit spectroscopy data for the interacting pairs AM 2306-721 and AM 2322-821 with grids of photoionization models found shallower metallicity gradients than the ones in isolated spiral galaxies. However, two works carried out the first systematic investigations about metallicity gradients in interacting galaxies. (a) Kewley et al. (2010) determined the metallicity gradients for eight galaxies in close pairs and found them shallower than gradients in isolated spiral galaxies. (b) Sánchez et al. (2014), using data obtained from the CALIFA survey, found that galaxies with evidence of interactions and/or clear merging systems present a significant shallower gradient.

Furthermore, the gas motions produced by the interactions also induced star formation along the disk of the galaxies involved (Alonso et al. 2012), and this burst of star formation may be associated with a flatter metallicity gradient (Kewley et al. 2010). For example, Chien et al. (2007) determined the oxygen abundance of 12 young star clusters in the merging galaxy pair NGC 4676. These authors found a nearly flat oxygen distribution along the northern tail of this object, suggesting efficient gas mixing (see also Bastian et al. 2009; Trancho et al. 2007). Recently, Scudder et al. (2012), using a large sample of galaxy pairs taken from the Sloan Digital Sky Survey Data Release 7, found that galaxies in pairs show a star formation rate (SFR) about 60% higher than the one in non-pair galaxies (see also Nikolic et al. 2004; Lambas et al. 2003; Barton et al. 2000). Additional analysis of these data by Ellison et al. (2013), who investigated the effects of galaxy mergers throughout the interaction sequence, revealed an enhancement of the average central SFR by a factor of about 3.5 in relation to the one in objects with no close companion. Ellison et al. (2013) also found a stronger deficit in the gas phase metallicity in the post-merger sample than in closest pairs (see also Alonso et al. 2012; Barton et al. 2000; Bernloehr 1993; Bergvall et al. 2003; Lambas et al. 2003; Di Matteo et al. 2008; Patton et al. 2011; Freedman Woods et al. 2010; Mihos et al. 2010).

Although recent efforts in the direction to understand the effects of interactions on chemical evolution of galaxies have been done (Krabbe et al. 2008; Kewley et al. 2010; Krabbe et al. 2011; Bresolin et al. 2012; Torres-Flores et al. 2014), the number of galaxies in close pairs for which the metallicity have been estimated along their galactic disks is insufficient for a statistical analysis. To increase the number of determinations of metallicity

gradients in galaxy pairs producing a better knowledge of the several phenomena that arise during the interactions is the main goal of this paper.

In a previous work (Krabbe et al. 2014, hereafter Paper I), we presented an observational study of the impact of the interactions on the electron density of H II regions located in seven systems of interacting galaxies. We found that the electron density estimates obtained in our sample are systematically higher than those derived for isolated galaxies. In the present paper, we mainly use these data to estimate the metallicity gradients along the disks of eight galaxy pairs. This work is organized as follows. In Section 2 we summarize the observations and data reduction. In Sect. 3 the method to compute the metallicity of the gas phase of our sample is described. Results and discussion are presented in Sections 4 and 5, respectively. The conclusions of the outcomes are given in Section 6.

2 OBSERVATIONAL DATA

We have selected eight close pairs systems from Ferreiro & Pastoriza (2004) to study the effects of minor mergers on gradient abundances of the individual galaxies. Objects with mass ratio in the range of $0.04 < M_{secondary}/M_{primary} < 0.2$, apparent B magnitude higher than 18, redshift in the range $0.01 \lesssim z \lesssim 0.06$, and classified as close interacting pairs were selected.

Long-slit spectroscopic data of the galaxy systems AM1054-325, AM 1219-430, AM 1256-433, AM 2030-303, AM 2058-381, AM 2229-735, AM 2306-721, and AM 2322-821 were obtained with the Gemini Multi-Object Spectrograph (GMOS) attached to the 8m Gemini South telescope. Spectra in the range 4400Å-7300Å were acquired with the B600 grating, a slit width of 1 arcsec and a spectral resolution of ~ 5.5 Å. Except for AM 2030-303, detailed information on the galaxy systems observed, containing most of the slit positions for each system and a complete description of the data reduction were presented in Paper I, and are not reproduced here.

AM 2030-303 is the only object in our sample that was not included in Paper I and its main information is presented in Table 1. For the systems AM 1256-433 and AM 2058-381 one more slit position than the ones presented in Paper I is considered in the present work (PAs 70° and 28°, respectively). It is important to note that for some systems of galaxies (e.g. AM 2306-721 and AM 2322-821, see Krabbe et al. 2008, 2011) we had spectra in the range of about 3400Å-7300Å. However, in order to obtain homogeneous metallicity determination,

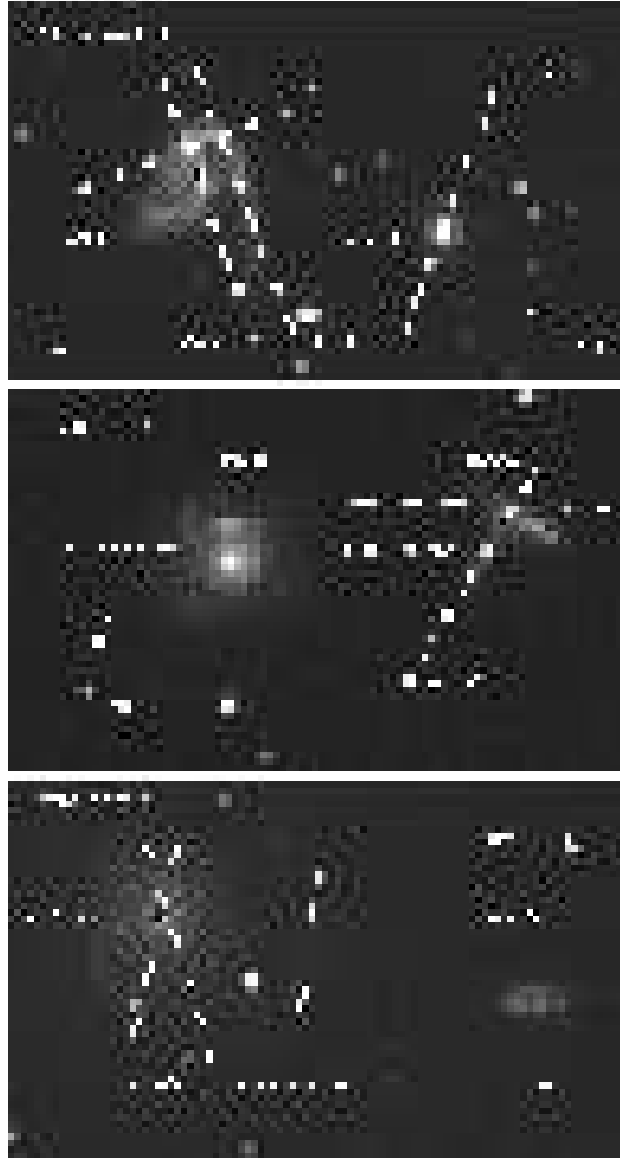


Figure 1. Slit positions for AM 1219-430, AM 2030-303 and AM 2322-821 systems superimposed on the GMOS-S r' acquisition images.

we restricted the analysis to the same wavelength range (i.e 4400\AA - 7300\AA). In Figure 1 the slit positions for these three systems are shown superimposed on the GMOS-S r' acquisition image (see Figure 1 of Paper I for the slit positions of the other five objects). These data were not included in Paper I due to the low signal-to-noise ratio (S/N) of the $[\text{S II}]\lambda 6716, \lambda 6731$ emission lines needed to perform the electron density estimations. The observed spectra comprise the flux contained in an aperture of $1 \text{ arcsec} \times 1.152 \text{ arcsec}$ which, considering a spatially flat cosmology with $H_0 = 71 \text{ kms}^{-1}\text{Mpc}^{-1}$, $\Omega_m = 0.270$, $\Omega_{\text{vac}} = 0.730$ (Wright 2006) and the distances to the systems of our sample, corresponds to apertures between about 200 and 1100 pc on the plane of the galaxies. Therefore, the physical properties derived from

Table 1. Morphological type, right ascension, declination, radial velocity, magnitude, and cross-identifications for AM 2030-303.

ID	Morphology	α (2000)	δ (2000)	cz (km/s)	m_B (mag)	Others names
AM 2030-303	SA? [2]	20 33 56.3	−30 22 41	12 323 [2]	15.25 [1]	ESO 463-IG 003 NED01
	G Trpl [1]	20 33 59.7	−30 22 29	12 465 [2]	17.80 [1]	ESO 463-IG 003 NED02
	G Trpl [1]	20 33 59.7	−30 22 23	12 474 [2]	21.39 [1]	ESO 463-IG 003 NED03

References: [1] Ferreiro & Pastoriza (2004); [2] Donzelli & Pastoriza (1997); Conventions: α , δ : Equatorial Coordinates.

Table 2. Nuclear separation (NS) between the galaxies of the pairs, galactocentric distance with surface brightness of 25 mag arcsec^{−2} (R_{25}), inclination angle (i), and the radial velocity (cz) of the objects in our sample.

ID		NS (kpc)	R_{25} (kpc)	i (°)	cz (km s ^{−1})
AM 1054-325	A	-	6.98 [3]	62 [2]	3 788
	B	17	6.81 [3]	54 [2]	3 850
AM 1219-430	A	-	15.3 [6]	50 [6]	6 957
	B	33.7	6.2 [6]	-	6 879
AM 1256-433	A	-	-	36 [2]	9 215
		-	-	33 [2]	9 183
	B	91.6	24.32 [4]	77 [4]	9 014
AM 2030-303	A	-	17.4 [4]	23 [4]	12 323
		-	-	-	12 465
	B	40.5	13.5 [4]	35 [4]	12 474
AM 2058-381	A	-	34.3 [4]	68 [4]	12 383
	B	44	16.7 [4]	57 [4]	12 460
AM 2229-735	A	-	26.1 [4]	60 [4]	17 535
	B	24.5	22.5 [4]	48 [4]	17 342
AM 2306-721	A	-	24.3 [4]	56 [5]	8 919
	B	52.6	15.6 [4]	60 [5]	8 669
AM 2322-821	A	-	13.5 [4]	20 [1]	3 680
	B	33.7	4.2 [4]	63 [1]	3 376

References [1] Krabbe et al. (2011); [2] Paturel et al. (2003); [3] Paturel et al. (1991); [4] Ferreiro et al. (2008), [5] Krabbe et al. (2008), [6] Hernandez-Jimenez et al. (2013).

these spectra represent the ones of a complex of H II regions. In Table 2 we present the nuclear separation between the components of the galaxy pairs, the galactocentric distances given in units of R/R_{25} , where R_{25} is the B-band isophote at a surface brightness of 25 mag arcsec^{−2}, the inclination angle (i) of each galaxy analysed, and the references from which the information was taken. The inclination of each galaxy with respect to the plane of the sky was computed as $\cos(i) = b/a$, where a and b are the major and minor semi-axes of the galaxy, respectively. The a and b values as well as the position angle of the major axis of each galaxy were obtained from the Gemini acquisition images in the r filter, using a simple isophotal fitting with the IRAF STSDAS.ELLIPSE task. The same procedure was used in Krabbe et al. (2011).

It can be seen in Tables 1 and 2 that some galaxies of our sample have large inclinations

and it could affect the derived abundance gradients. In fact, as pointed out by Sánchez et al. (2012), face-on galaxies are more suitable to study the spatial distribution of the properties of H II regions. For example, if we assume an inclination angle i for a given galaxy larger than the real one, the abundance gradient derived would be steeper than the one obtained with the right i value. However, this effect is critical for isolated spiral galaxies which have a clear (or steep) abundance gradients and it is not so important for objects with shallow gradients, such as interacting galaxies.

To obtain the nebular spectra not contaminated by the stellar population contribution, we use the stellar population synthesis code STARLIGHT (Cid Fernandes et al. 2005) following the methodology presented in Krabbe et al. (2011). Detailed analysis of the stellar population for the sample of objects will be presented in a future work (Rosa et al. in preparation). Once the stellar population contribution has been determined, the underlying absorption line spectrum was subtracted from the observed spectra. In Fig. 2 the spectrum of the region with the highest brightness of AM 1256-433 along the PA=325°, the synthesized spectrum and the pure emission spectrum corrected for reddening are shown. The intensities of the emission-lines H β , [O III] λ 5007, H α , [N II] λ 6584, and [S II] λ 6716, λ 6731 were obtained from the pure nebular spectrum of each aperture using Gaussian line profile fitting.

We used the IRAF¹ SPLOT routine to fit the lines, with the associated error given as $\sigma^2 = \sigma_{cont}^2 + \sigma_{line}^2$, where σ_{cont} and σ_{line} are the continuum rms and the Poisson error of the line flux, respectively. The residual extinction associated with the gaseous component for each spatial bin was calculated comparing the observed value of H α /H β ratio to the theoretical value 2.86 obtained by Hummer & Storey (1987) for an electron temperature of 10 000 K and an electron density of 100 cm⁻³. This value for the electron density is in the range of mean electron density values ($24 \lesssim N_e \lesssim 532$ cm⁻³) found for interacting galaxies in Paper I. The correction for foreground dust was done using the reddening law given by Cardelli et al. (1989), assuming the specific attenuation $R_V = 3.1$. We considered only emission-line measurements whose S/N was higher than 8. The galactocentric distance in relation to R_{25} , the flux of H β , the extinction coefficient $C(\text{H}\beta)$, and the emission-line intensities normalized to the flux of H β for the regions considered in the systems are presented in Table 3.

¹ Image Reduction and Analysis Facility, distributed by NOAO, operated by AURA, Inc., under agreement with NSF.

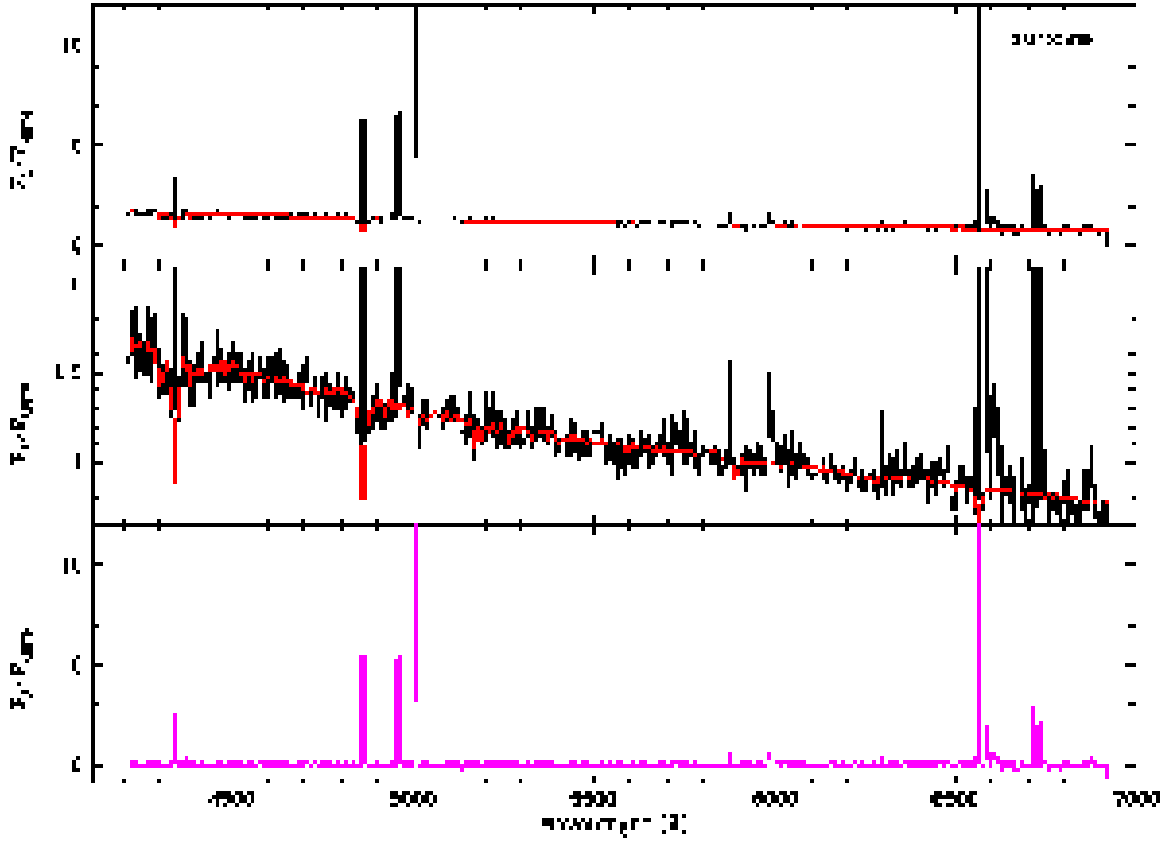


Figure 2. Stellar population synthesis for the brightest region of AM 1256B along the PA=325°. Top panel: reddening-corrected spectrum (black line) and the synthesized spectrum (red line). Middle panel: y-axis zoom of the top panel. Bottom panel: pure emission spectrum obtained as the difference between both spectra in top panel.

Table 3. Specific parameters and intensity of emission lines corrected by reddening (relative to $H\beta=100$). Only the AM 1054B galaxy is shown here. The total list of galaxies is available in electronic form.

R/R_{25}	$\log[F(H\beta)]^*$	$C(H\beta)$	[OIII] λ 5007	H α	[NII] λ 6584	[SII] λ 6716	[SII] λ 6731
AM 1054B							
0.00	−14.51	0.40	152±27	278±9	112±6	24±10	27±7
0.04SW	−14.97	0.26	154±22	281±7	115±5	28±4	29±4
0.04NE	−14.93	0.23	141±21	282±9	114±6	37±3	37±7
0.08NE	−15.82	0.08	139±11	285±11	119±8	—	—
0.13NE	−17.11	0.08	113±19	285±15	119±11	—	—

[*] Logarithm of the $H\beta$ observed flux in $\text{erg s}^{-1} \text{cm}^{-2}$.

3 DETERMINATION OF THE OXYGEN ABUNDANCE GRADIENTS

Since emission-line sensitive to the electron temperature are not detected in the spectra of the objects in our sample, the metallicity of the gas phase, traced by the relative abundance of the oxygen to the hydrogen (O/H), was estimated using calibrations based on strong emission-lines.

Considering the emission-lines observed in our sample, it is only possible to use the in-

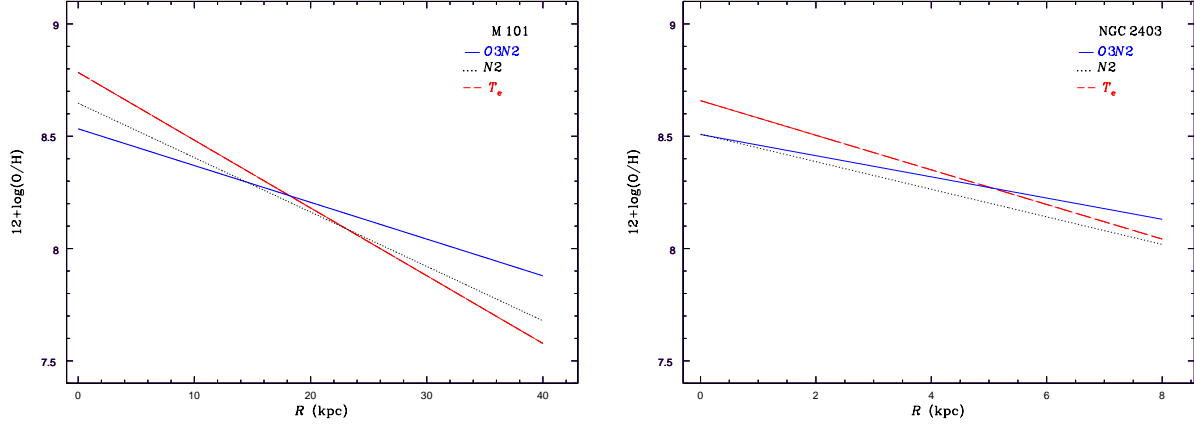


Figure 3. Oxygen abundance gradients computed via the $N2$, $O3N2$ indexes and direct estimations of the oxygen electron temperatures for the galaxies M 101 (left) and NGC 2403 (right) using data taken from Kennicutt et al. (2003) and Garnett et al. (1997), respectively.

tensities of the emission-lines defined as $N2 = \log([N II]\lambda 6584 / H\alpha)$ and $O3N2 = \log([([O III]\lambda 5007 / H\beta) / ([N II]\lambda 6584 / H\alpha)])$ proposed by Storchi-Bergmann et al. (1994) and Alloin et al. (1979), respectively, as O/H indicators. We used the relations among these indexes and the O/H , calculated using direct estimations of the oxygen electron temperatures (T_e -method), proposed by Pérez-Montero & Contini (2009) and given by

$$12 + \log(O/H) = 0.79 \times N2 + 9.07 \quad (1)$$

and

$$12 + \log(O/H) = 8.74 - 0.31 \times O3N2. \quad (2)$$

These calibrations are very similar to the ones proposed by Pettini & Pagel (2004). Most recent update of this calibration was done by Marino et al. (2013), who used direct oxygen abundance measurements obtained from CALIFA survey and other sources from the literature. López-Sánchez & Esteban (2010), using multiwavelength analysis of a sample of starburst galaxies and data compiled from the literature, showed that the $N2$ and $O3N2$ parameters provided acceptable results for objects with $12 + \log(O/H) > 8.0$. López-Sánchez & Esteban (2010) also found that empirical calibrations considering these indexes give results that are about 0.15 dex higher than the oxygen abundances derived via the T_e -method. Despite this difference is similar to the uncertainties of oxygen abundances derived from the T_e -method (e.g. Hägele et al. 2008; Kennicutt et al. 2003), it seems to vary with the regime of metallicity (Dors et al. 2011). This can yield steeper oxygen gradients than the ones from the T_e -method or erroneous bend in the slope of abundance gradients (Pilyugin 2003). With the goal to compare O/H gradients derived using the $N2$ and $O3N2$

Table 4. Slope of the oxygen abundance gradient and the central value derived for the objects in our sample with no bi-modal gradient behaviour.

Object	<i>N2</i>		<i>O3N2</i>	
	Slope [dex/(R/R_{25})]	$12+\log(\text{O}/\text{H})_{\text{Central}}$	Slope [dex/(R/R_{25})]	$12+\log(\text{O}/\text{H})_{\text{Central}}$
AM 1054B	$+0.11 \pm 0.04$	8.54 ± 0.01	$+0.36 \pm 0.04$	8.75 ± 0.06
AM 1219B	$+0.10 \pm 0.18$	8.89 ± 0.04	—	—
AM 2058A	-0.29 ± 0.08	8.79 ± 0.02	-0.35 ± 0.08	8.78 ± 0.02
AM 2229A	$+0.03 \pm 0.09$	8.71 ± 0.03	-0.11 ± 0.06	8.70 ± 0.02
AM 2306A	-0.40 ± 0.05	8.81 ± 0.02	-0.57 ± 0.06	8.83 ± 0.02
AM 2322A	-0.17 ± 0.01	8.79 ± 0.01	-0.18 ± 0.02	8.77 ± 0.01
AM 2322B	-0.14 ± 0.05	8.57 ± 0.02	-0.07 ± 0.05	8.53 ± 0.02

indexes with the ones obtained from the T_e -method, we used data of H II regions located along the disks of the spiral galaxies M 101 e NGC 2403 obtained by Kennicutt et al. (2003) and Garnett et al. (1997), respectively. In Fig. 3 these gradients are shown, where we can see gradients derived from the indexes are somewhat shallower than the ones from T_e -method.

Scarano et al. (2011) and Bresolin et al. (2012) pointed out that gradients are less affected by uncertainties in oxygen estimations yielded by calibration of strong emission-lines. However, it can be seen in Fig. 3 that the value of the O/H extrapolated for the central region of the galaxies ($R = 0$), obtained using different methods, can differ by until 0.4 dex. This difference is higher than the uncertainty attributed to the O/H estimations using strong emission-line calibrations (Kewley & Ellison 2008). Similar results were found by Bresolin (2011) comparing the oxygen gradient for NGC 4258 using theoretical calibrations by McGaugh (1991) and empirical ones by Pilyugin & Thuan (2005). The latter provides results essentially in consonance with those obtained from the T_e -method (see also Pilyugin et al. 2012).

4 RESULTS

In Figs. 4-11 the oxygen abundance determinations along the disks of the galaxies of our sample, obtained using Eqs. 1 and 2, and linear regression fits to these data are presented. In Table 4 the slopes of these fits and the values of $12+\log(\text{O}/\text{H})$ central ($R = 0$) for the galaxies which only a global gradient represents well the O/H disk distribution (i.e. no bi-modal gradient behaviour were derived) are presented. It can be noted that in most cases, shallow gradients are derived in the interacting galaxies. The average values of the global

gradients calculated for the close pairs in our sample are -0.10 ± 0.19 [dex/(R/R_{25})] and -0.15 ± 0.31 [dex/(R/R_{25})] using the $N2$ and $O3N2$ indexes, respectively. These values are in consonance with the mean gradient -0.25 ± 0.02 [dex/(R/R_{25})] derived by Kewley et al. (2010) and they are shallower than the mean metallicity gradient -0.57 ± 0.19 [dex/(R/R_{25})] derived for 11 isolated spiral galaxies by Rupke et al. (2010b). Sánchez et al. (2014), using the CALIFA data survey, presented a study of galaxies with different interaction stages in order to study the effect on the abundance gradient. This study has a stronger statistical significance than the one in previous studies. Sánchez et al. (2014) showed the distribution of slopes of the abundance gradients derived for the different classes based on the interaction stages. From this analysis, Sánchez et al. (2014) found that galaxies with not evidence of interaction have an average value for the gradient of -0.11 dex/ r_e and objects with evidence for early or advanced interactions have a slope of -0.05 dex/ r_e , being r_e the disk effective radius. This result confirms the our findings and the ones obtained by Kewley et al. (2010). In what follows, the results obtained for each system are discussed separately.

4.1 AM 1054-325

This system is composed by two galaxies, one main galaxy namely AM 1054A and other secondary AM 1054B. Using the diagnostic diagram $[O\text{ III}]\lambda 5007/H\beta$ versus $[O\text{ I}]\lambda 6300/H\alpha$, we found (see Paper I) that almost all H II regions located in the disk of AM 1054A have emission lines excited by shock gas. Therefore, abundance determinations was not performed for this object since shocks alter the ionization in a way that the abundance calibrators can not be used due to they are calibrated for H II regions dominated by photoionization by young stars.

In Fig. 4 the O/H distribution versus the galactocentric radius R normalized by R_{25} for AM 1054B is shown. We found gradient slopes of 0.11 ± 0.04 and 0.36 ± 0.04 dex/(R/R_{25}), with the central $12+\log(O/H)$ value being $8.54 (\pm 0.01)$ and $8.75 (\pm 0.06)$ dex from the $N2$ and $O3N2$ indexes, respectively. AM 1054B is the only object in our sample for which both estimations of the central oxygen abundances are not in agreement among themselves within the errors (see Table 4). However, as can be seen in Fig. 4, the slopes were obtained using few points. Hence, the gradient determination is highly uncertain, although the current data indicate a flat O/H distribution.

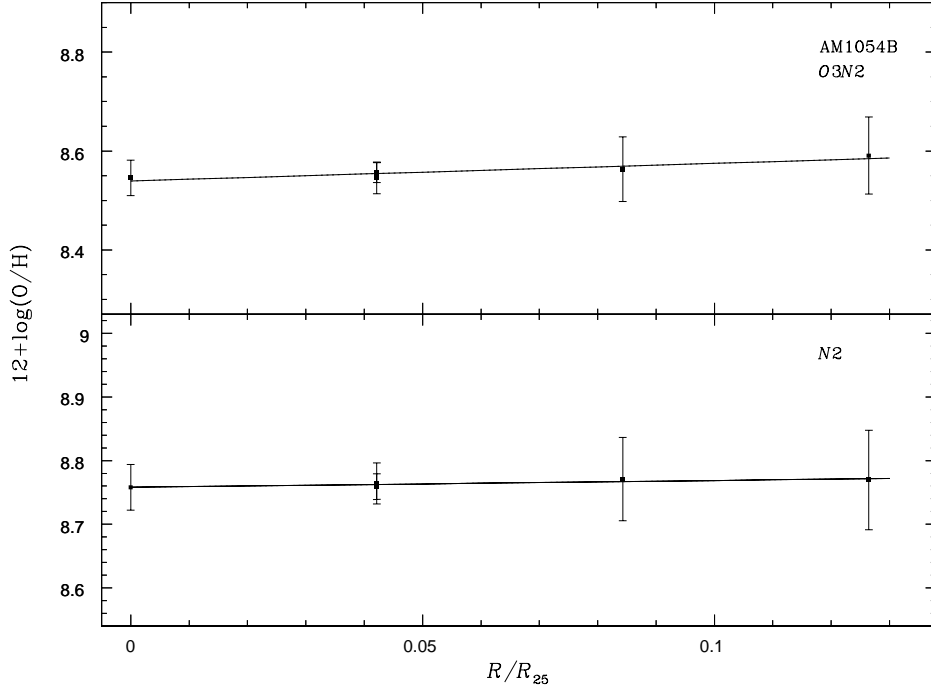


Figure 4. Oxygen abundance estimations along the disk of AM1054B vs. the galactocentric distance given in R/R_{25} . Points represent oxygen estimations obtained via the $N2$ (lower panel) and $O3N2$ (upper panel) indexes. Lines represent a linear regression fit to our estimations whose coefficients are given in Table 4.

4.2 AM 1219-430

This system is composed by the main galaxy AM 1219A and a secondary galaxy, AM 1219B. Since it was not possible to measure the $[\text{O III}]\lambda 5007$ emission line with enough S/N in our spectrum of AM 1219B, for this object O/H was estimated only using $N2$. We corrected by inclination the galactocentric distances for the main galaxy AM 1219A considering $i=50^\circ$.

In Fig. 5 the O/H distribution in both galaxies are shown. For AM 1219B we derived a slope $+0.10 \pm 0.18$ and a central oxygen abundance of 8.89 ± 0.04 dex. Such as for AM 1054B, the slope for AM 1219B was derived with few points (and with a large dispersion), which does the result highly uncertain. For AM 1219A the estimated oxygen gradient slopes are -0.29 ± 0.04 and -0.54 ± 0.04 using the $N2$ and $O3N2$ indexes, respectively, with a central value of $12+\log(\text{O}/\text{H}) \sim 8.8$ derived from both indexes. For values of R/R_{25} from about 0.4 to 0.5, we can see a larger dispersion in the oxygen distribution than the one found at other galactocentric distances. Regions at this distance range, as can be seen in Fig. 1, are located in the intersections of the slits and are regions with high surface brightness. It can be noted in Fig. 5, for AM 1219A, that there is a change in the slope at about $R/R_{25} = 0.5$. The slopes of the abundance gradient in the inner disk ($R/R_{25} < 0.5$) considering the $O3N2$ and $N2$

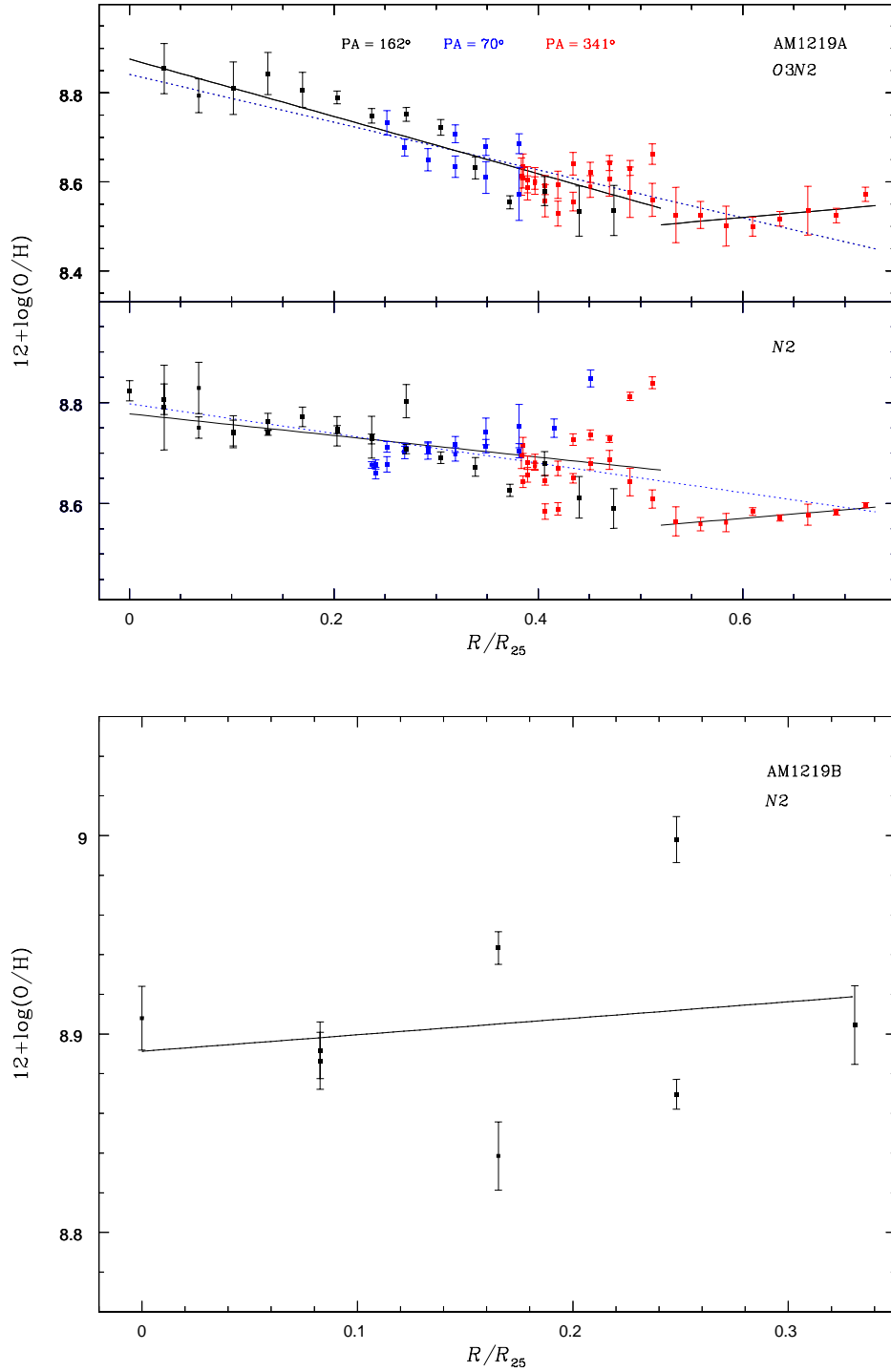


Figure 5. Same as Fig. 4 but for AM1219A and AM1219B. For AM1219A, determinations for the regions observed in different long-slit positions are indicated for distinct colours, as indicated. Also, linear regressions considering all regions along the disk (dotted blue line) and inner and outer regions to galactocentric distance $R/R_{25}=0.5$ (solid black line) are shown.

indexes are -0.64 ± 0.05 and -0.21 ± 0.05 , respectively. For the outer region ($R/R_{25} > 0.5$), the slopes are $+0.20 \pm 0.11$ and $+0.16 \pm 0.11$ using $O3N2$ and $N2$, respectively.

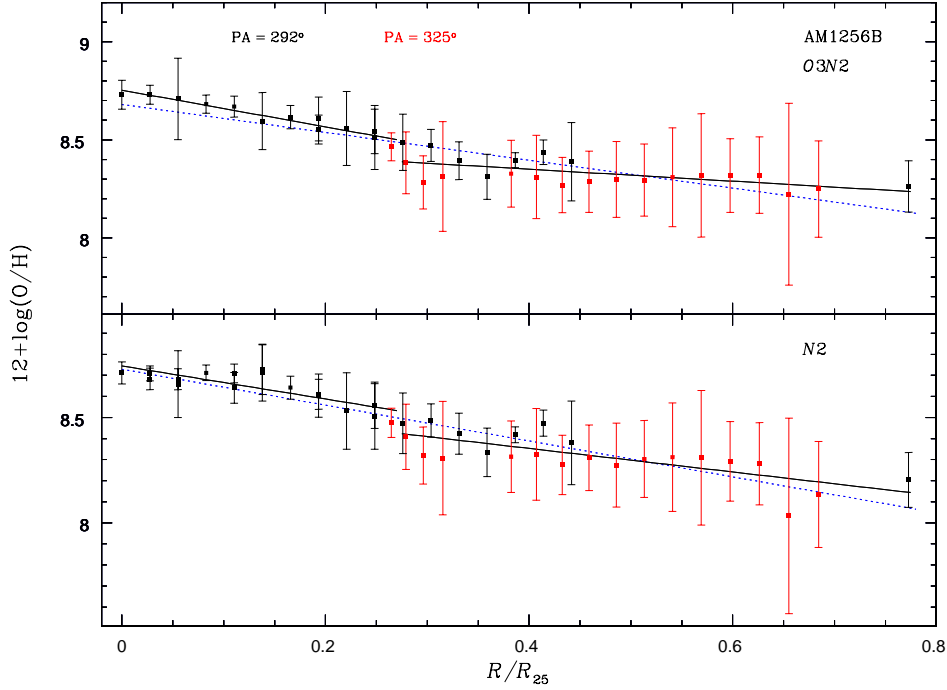


Figure 6. Same as Fig. 5 but for AM1256B. Linear regressions considering all regions along the disk (dotted blue line) and inner and outer regions to galactocentric distance $R/R_{25}=0.35$ (solid black line) are shown.

4.3 AM 1256-433

As was reported in Paper I, the AM 1256-433 system is composed by three galaxies and we only observed the AM1256-433B component. For this object, the galactocentric distance measurements were corrected by inclination considering $i=77^\circ$. In Fig. 6 the O/H distribution via the $N2$ and $O3N2$ indexes are shown. We obtained gradient slopes of -0.85 ± 0.06 and -0.71 ± 0.06 for these indexes, respectively, with a central $12+\log(\text{O}/\text{H})$ value of ~ 8.7 dex. Interestingly, we can note a steeper oxygen gradient for $R/R_{25} < 0.27$ than the one obtained for the outer regions. The slopes of the abundance gradient in the inner disk considering the $N2$ and $O3N2$ indexes are -0.78 ± 0.13 and -0.93 ± 0.07 . For the outer disk ($R/R_{25} > 0.27$) we derived for $N2$ and $O3N2$ indexes the slopes -0.55 ± 0.10 and -0.30 ± 0.08 , respectively. The slopes of the global fits to the abundance estimations are dominated by the values of the outer regions of the galaxy, and they are slightly steeper than the ones obtained only considering these outer regions.

4.4 AM 2030-303

This system is composed by three galaxies, a main galaxy AM2030A (ESO 463-IG 003 NED01), the ESO 463-IG 003 NED02 and ESO 463-IG 003 NED03. These last two objects

are a sub-system namely AM 2030B. In Fig. 1 the slit positions for each object is shown. We corrected by inclination the galactocentric distances of AM 2030B considering $i=35^\circ$. Due to the few number of H II regions observed, it was not possible to compute the O/H gradient for ESO 463-IG 003 NED002. In Fig. 7 the results for AM 2030A and B are presented.

For AM 2030A, considering a global fits, we obtained a central value $12+\log(\text{O}/\text{H})=8.73\pm0.10$ with a slope -0.31 ± 0.30 using $N2$ and 8.62 ± 0.07 and -0.22 ± 0.20 using $O3N2$. These values are similar to the highest O/H value obtained for the H II region CDT1 in NGC 1232 by Castellanos et al. (2002). Now, considering an abundance gradient break, the slopes for inner disk ($R/R_{25} < 0.27$) obtained via $N2$ and $O3N2$ indexes are -0.27 ± 0.46 and -0.95 ± 0.27 , respectively. For the outer disk ($R/R_{25} > 0.27$) we derived for $N2$ and $O3N2$ indexes the slopes -0.47 ± 0.01 and 0.00 ± 0.45 , respectively.

For AM 2030B (ESO 463-IG 003 NED003) we found two different O/H abundance distributions at the inner and the outer regions of $R/R_{25}=0.2$. The slopes of the abundance gradient in the inner disk ($R/R_{25} < 0.17$) considering the $N2$ and $O3N2$ indexes are $+1.85\pm0.43$ and $+0.92\pm0.22$, respectively. For the outer disk ($R/R_{25} > 0.17$) we derived for $N2$ and $O3N2$ indexes the slopes -0.28 ± 0.25 and -0.17 ± 0.18 , respectively.

4.5 AM 2058-381

For this system the O/H gradient was only determined for one galaxy, AM 2058A, since the H II regions of its companion galaxy, AM 2058B, have emission lines excited by gas shock (see Paper I). In Fig. 8 the oxygen distribution is shown, where the galactocentric distances were corrected considering $i=68^\circ$. We found a slope for the O/H gradient from the $N2$ index of -0.29 ± 0.08 with $12+\log(\text{O}/\text{H})=8.79\pm0.02$ for the central region. Using the $O3N2$, we found -0.35 ± 0.08 and 8.78 ± 0.02 dex.

4.6 AM 2229-735

We obtained the O/H abundance distributions only for the main galaxy of the system AM 2229-735, namely AM 2229A and these are shown in Fig. 9. Galactocentric distances in this object were corrected by inclination considering $i=48^\circ$. For estimations via the $N2$ index we found a slope of 0.03 ± 0.09 with central oxygen abundance $12+\log(\text{O}/\text{H})=8.71\pm0.03$ dex. For the $O3N2$ index these values are -0.11 ± 0.06 and 8.70 ± 0.02 dex.

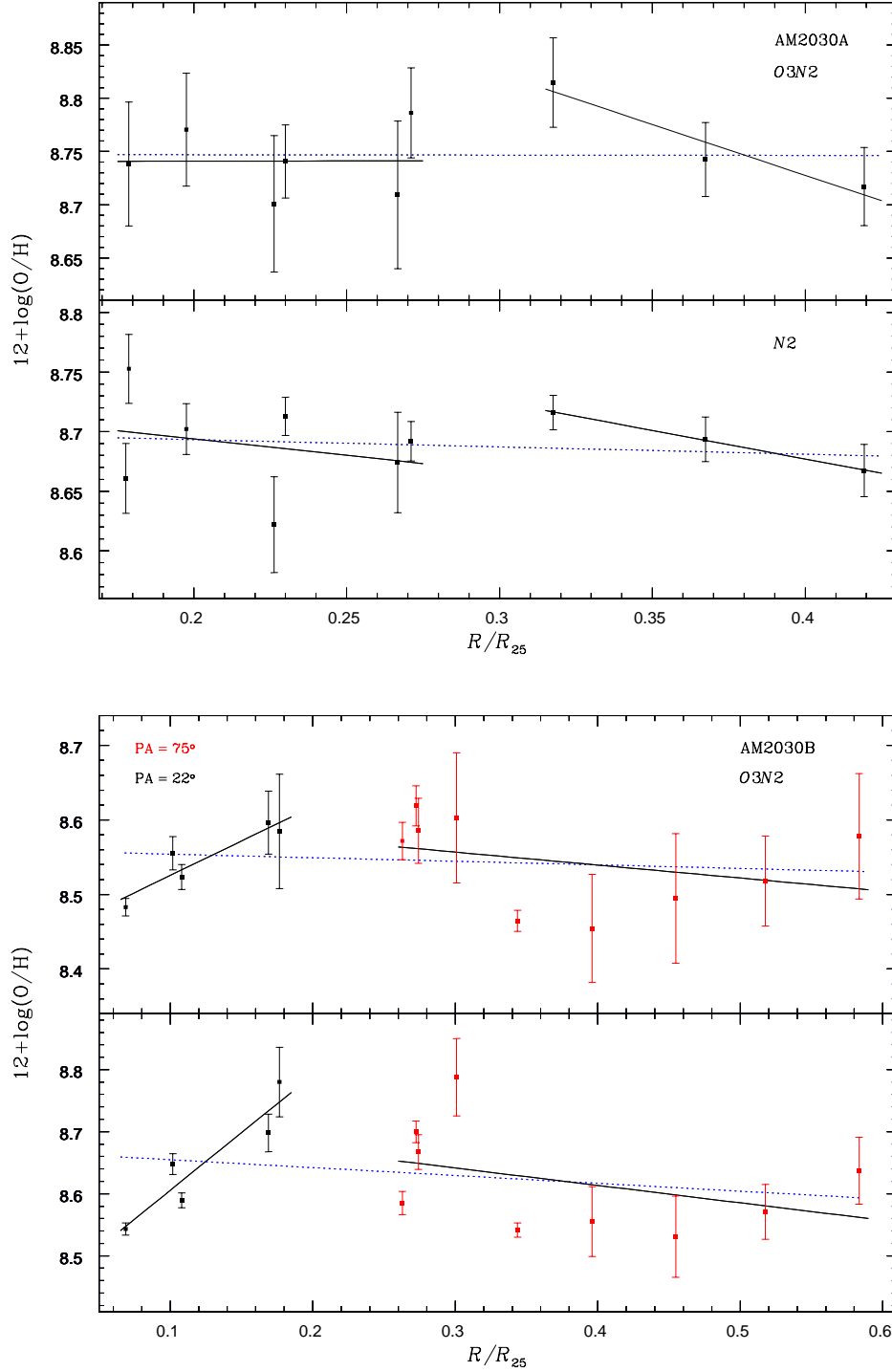


Figure 7. Same as Fig. 5 but for AM2030A and AM2030B (ESO 463-IG 003 NED003). Linear regressions considering all regions along the disk (dotted blue line) and inner and outer regions to galactocentric distance $R/R_{25}=0.2$ (solid black line) are shown.

4.7 AM 2306-721

This pair is composed by a main galaxy AM2306A and a companion galaxy AM2306B. The O/H gradient (see Fig. 10) was determined only for the main galaxy AM2306A because,

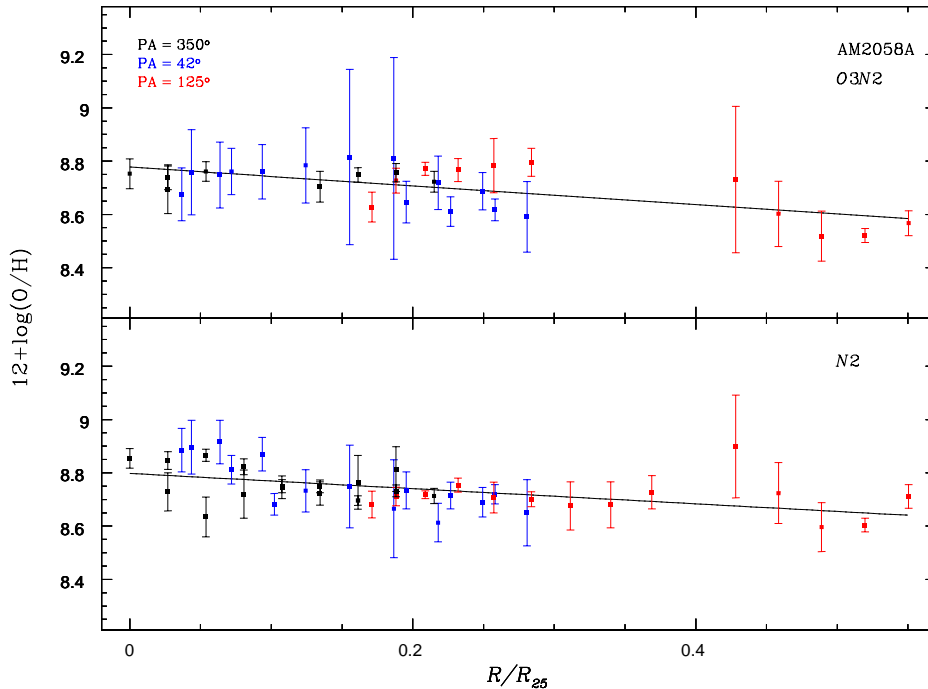


Figure 8. Same as Fig. 5 but for AM2058A.

for its companion, AM2306B, the presence of gas shock excitation along the disk was found (see Paper I). We found by using the $N2$ index a slope of -0.40 ± 0.05 and a central value $12+\log(O/H)=8.81 \pm 0.02$ dex. Using the $O3N2$ index the values -0.57 ± 0.06 and 8.83 ± 0.02 dex were found.

4.8 AM2322-821

In Fig. 11 the O/H distributions along the disk of the pair of galaxies AM2322A and AM2322B are shown. For AM2322A a correction for inclination was performed considering $i=20^\circ$. For AM2322A we obtained by using the $N2$ index a slope of -0.17 ± 0.01 and a $12+\log(O/H)=8.79 \pm 0.01$ dex for the central part. From the $O3N2$ index, these values were found to be -0.19 ± 0.01 and 8.77 ± 0.01 dex. For the secondary object AM2322B, the use of the $N2$ yielded -0.14 ± 0.05 and 8.57 ± 0.20 dex for the central part, while the use of the $O3N2$ yielded -0.07 ± 0.05 and 8.53 ± 0.20 dex.

5 DISCUSSION

Determinations of the oxygen abundance gradients in interacting galaxies have showed that these are shallower than the ones in isolated galaxies. This result was obtained recently and

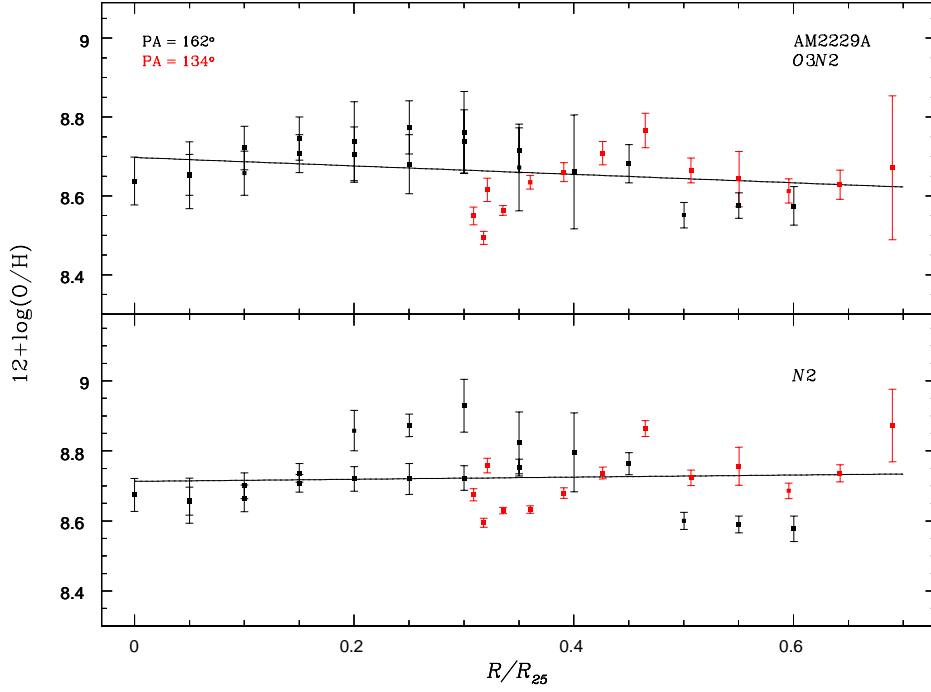


Figure 9. Same as Fig. 5 but for AM2229A.

few works have addressed this subject. In what follow some works in this directions are summarized.

(i) Krabbe et al. (2008) obtained long slit spectroscopy data with the Gemini/GMOS of the two components (A and B) of the galaxy pair AM2306-721. These authors used a comparison between the observed emission-line ratio intensities (R_{23} and $[\text{O II}]\lambda 3727/[\text{O III}]\lambda 5007$; see McGaugh 1991) and those predicted by photoionization models to determine the metallicity gradient. Krabbe and collaborators found a clear gradient for the most massive object of the pair, AM2306A, while for AM2306B an oxygen abundance relatively homogeneous across the disc was found.

(ii) Kewley et al. (2010) selected 5 sets of close pairs with separation between 15-25 kpc from the sample of Barton et al. (2000) and obtained spectra for 12-40 star-forming regions in 8 of the close pair galaxies with the Keck Low-Resolution Imaging Spectrograph. This work was the first systematic investigation about metallicity gradients in close pairs. Kewley et al. (2010) found that the metallicity gradients in their sample are significantly shallower than gradients in isolated spiral galaxies. They used a theoretical calibration between the $[\text{N II}]\lambda 6584/[\text{O II}]\lambda 3727$ emission-line ratio and the metallicity.

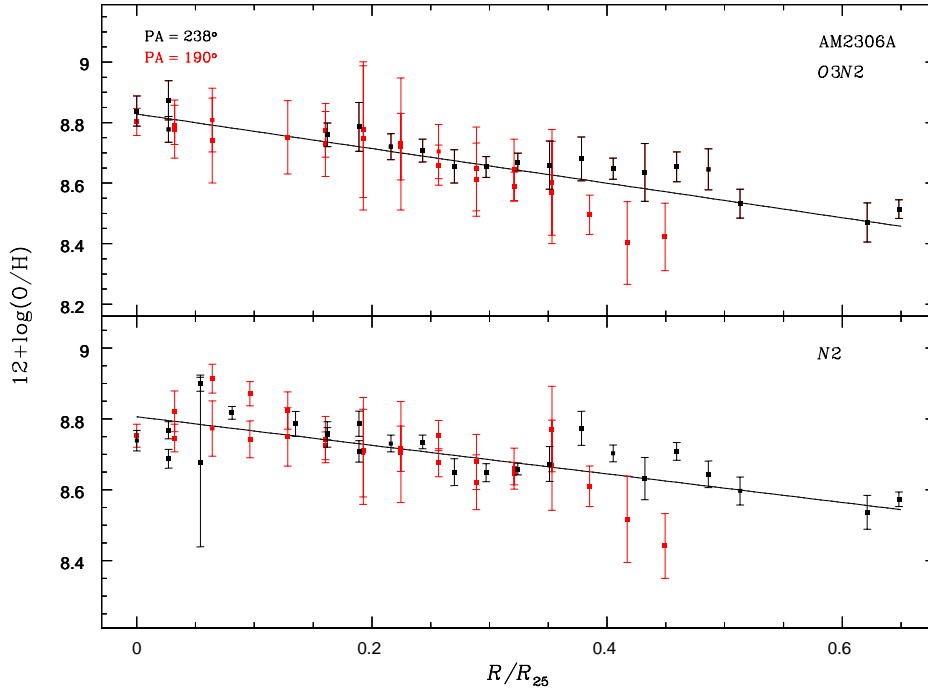


Figure 10. Same as Fig. 5 but for AM2306A.

(iii) Krabbe et al. (2011) obtained spectroscopic data of the two components (A and B) of the system AM 2322-821 with the Gemini/GMOS. The oxygen gradient was derived following the same procedure than in Krabbe et al. (2008) and a flat oxygen gradient was derived for both galaxies.

(iv) Bresolin et al. (2012), who used the Focal Optical Reducer and Spectrograph (FORS2) attached to the Very Large Telescope, obtained optical spectroscopy of H II regions belonging to NGC 1512. This galaxy has a companion, NGC 1510, separated by about 13.8 kpc. A flatten radial abundance gradient was also obtained by using several calibrations based on strong lines, as well as some oxygen abundance determinations using the T_e -method.

(v) Torres-Flores et al. (2014) obtained Gemini/GMOS spectroscopic data of the interacting galaxy NGC 92, which is part of a compact group and displays an extended tidal tail. Torres-Flores et al. (2014) used calibrations of the $N2$, $O3N2$ and $[Ar\ III]\lambda 7136/[O\ III]\lambda 5007$ indexes proposed by Pettini & Pagel (2004) and Stasińska (2006) to estimate the O/H abundance. Torres-Flores and collaborators found that most of the regions in NGC 92 present a similar oxygen abundance, which produces an almost flat metallicity gradient, with a possible break in this gradient for the galactocentric distance of ~ 10 kpc.

(vi) Most recently, Sánchez et al. (2014), based on the largest and better defined statistical sample of galaxies yielded by the CALIFA survey, compared the O/H abundance gradient

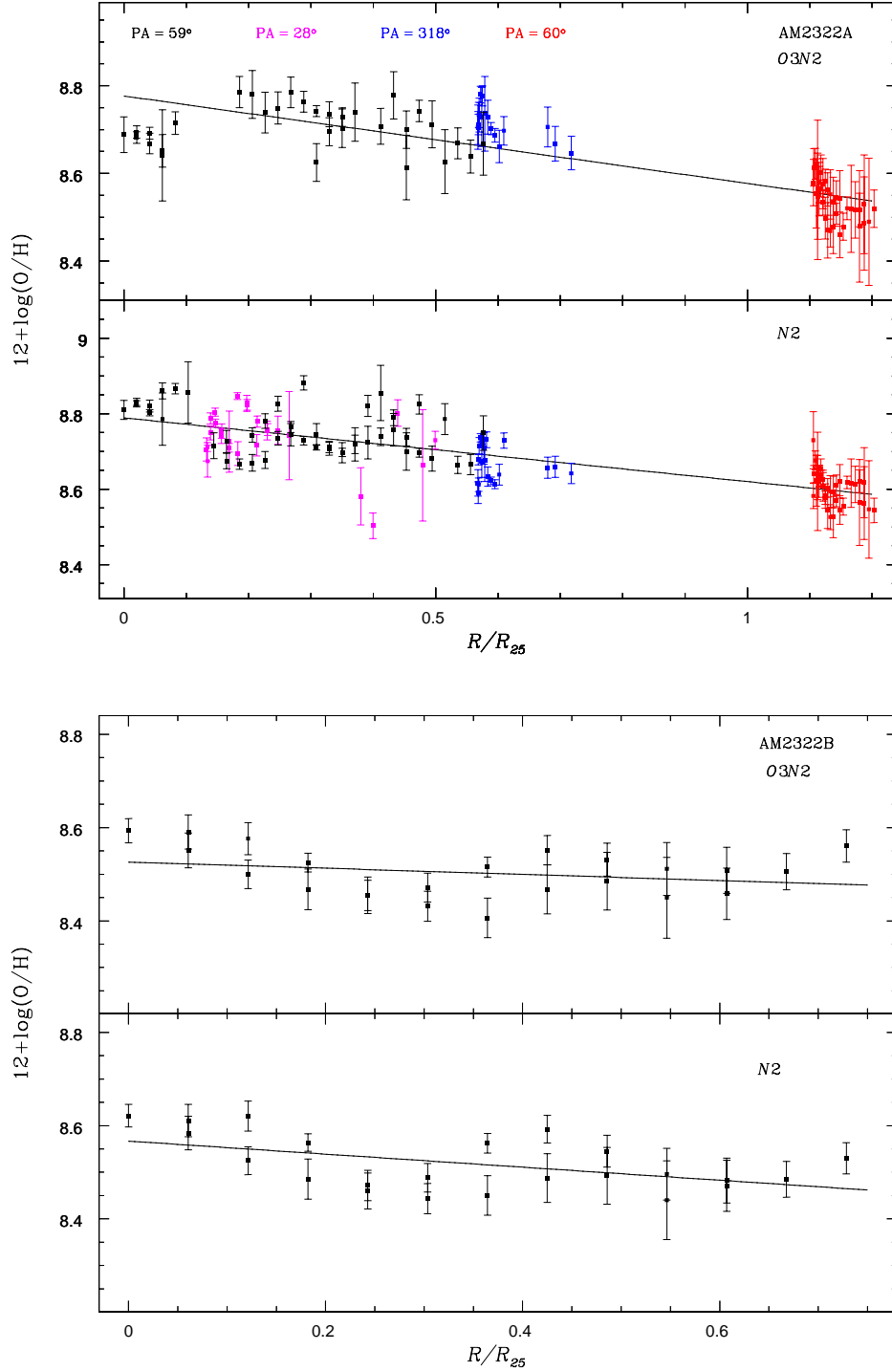


Figure 11. Same as Fig. 5 but for AM2322A and AM2322B.

of about 300 nearby galaxies, with more than 40 mergers/interacting systems, being half of them galaxy pairs. Sánchez et al. (2014) found, for the first time, a clear statistical evidence of a flattening in the abundance gradients in the interacting systems at any interaction stage, in agreement with the previous results.

From the literature summarized above it can be seen that oxygen gradients have been determined for close pairs or mergers systems mainly using different strong emission-line calibrations and some few determinations using the T_e -method. In this paper, we performed a new determination of the O/H gradients for the galaxies AM 2306A and AM 2322A-B previously studied by Krabbe et al. (2008, 2011) and presented an analysis of eight more galaxies in close pairs. In Fig. 12 the oxygen gradients from $N2$ derived for our sample, for the galaxies in the pairs from the literature cited above, and for four isolated ones, also from the literature, are shown. We can see that the oxygen gradients derived for the objects in our sample are shallower than the ones in isolated spirals. Although most of the slopes of these gradients are in consonance with the ones obtained by Kewley et al. (2010), we found lower O/H abundances for the central parts of the galaxies. This is due to the oxygen abundance estimations via theoretical calibrations, such as the one used by Kewley et al. (2010), yield higher values than the ones from calibrations based on oxygen estimations via T_e -method (see, for example, Dors & Copetti 2005). Krabbe et al. (2008), Kewley et al. (2010) and most recently, Sánchez et al. (2014), interpreted the absence of abundance gradient in interacting galaxies as being due to the mixing produced by low-metallicity gas from the outer parts with the metal-rich gas of the centre of the galaxy. Here we confirmed this result by increasing the sample of objects.

As we pointed out in Sect. 4, a flattening in the oxygen gradient was found in the outer part of AM 1256B from $R/R_{25} \approx 0.35$ ($R \approx 8.5$ kpc), AM 1219A from $R/R_{25} \approx 0.5$ ($R \approx 7.6$ kpc) and AM 2030B from $R/R_{25} \approx 0.2$ ($R \approx 2.7$ kpc). In the case of AM 1219A and AM 1256B the inner gradients have negative slopes while AM 2030B presents a positive inner gradient. In contrast, AM 2030A has a positive-slope outer gradient while the inner one is almost compatible with a flat behaviour, with the break at about $R/R_{25} \approx 0.3$ ($R \approx 5$ kpc). However, if we take into account the errors in the measurements, in the latter case the slope of the outer gradient is also compatible with zero, although due to the low number of H II regions in the outer zone we are not able to give a conclusion. The flattening in the oxygen gradients in the outer part were also found for either individual galaxies (Rosales et al. 2011; Torres-Flores et al. 2014; Bresolin et al. 2012; Marino et al. 2012; Miralles-Caballero et al. 2014; Martin & Roy 1994; Zahid & Bresolin 2011; Bresolin et al. 2009; Goddard et al. 2011; Rodríguez-Baras et al. 2014), a small sample of interacting galaxies (Werk et al. 2011), a large sample of objects (Sánchez et al. 2014, 2012), or even for the Milky Way (Esteban et al. 2013). Basically, there are four theoretical scenarios to explain

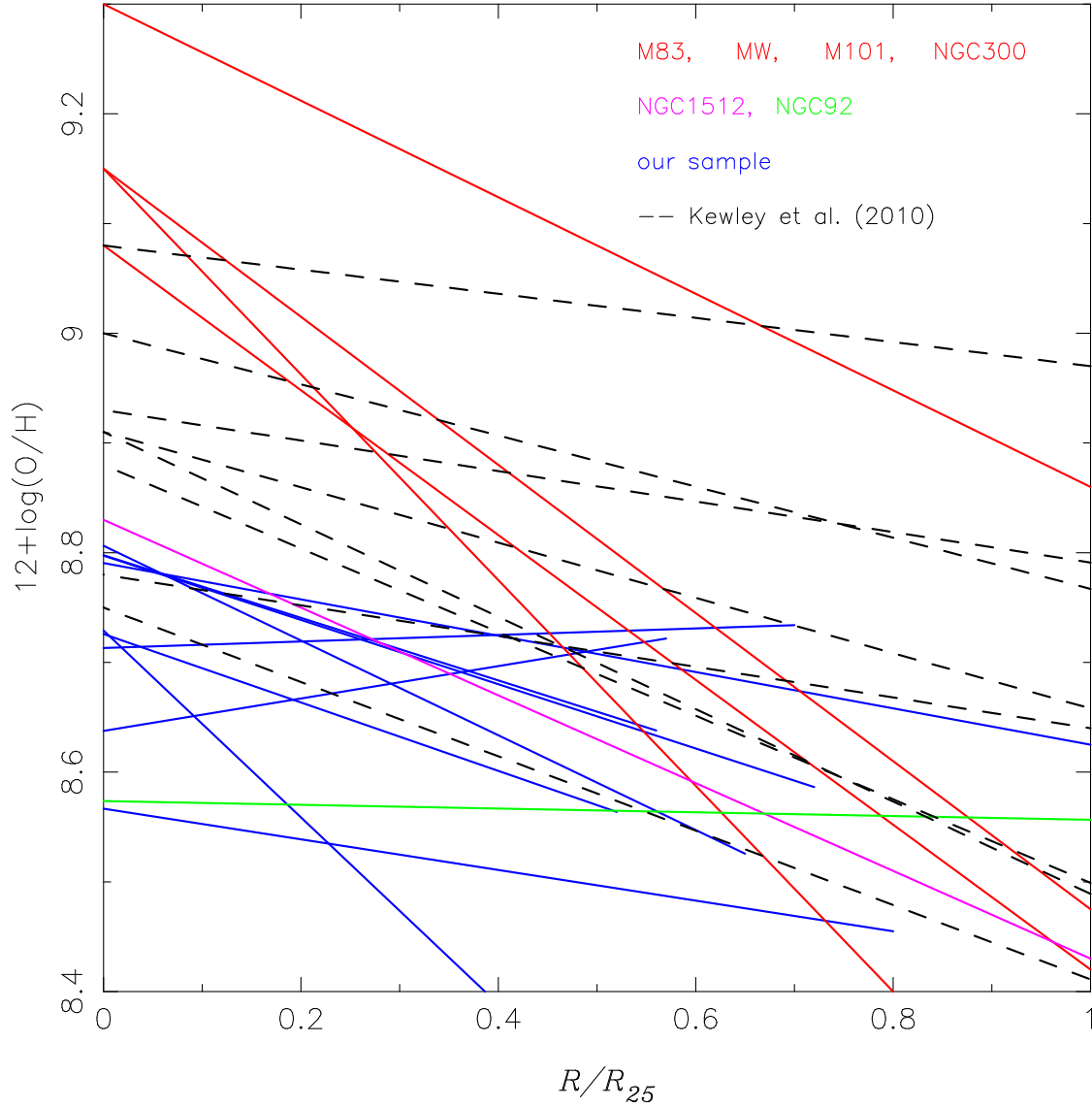


Figure 12. Metallicity gradients from $N2$ for our sample. The gradients for AM1219B and AM1054B, derived with few points (see text), are not shown. For comparison, we show the metallicity gradients for the isolated galaxies M101, Milk Way, M83, NGC300, whose the data were taken from Kennicutt et al. (2003), Shaver et al. (1983), Bresolin et al. (2005), and Bresolin et al. (2009), respectively; and eight interacting galaxies presented by Kewley et al. (2010), NGC92 (Torres-Flores et al. 2014) and NGC1512 (Bresolin et al. 2012).

the flattening of the oxygen abundance gradients at a given galactocentric distance. (i) The pumping out effect of corotation, which produces gas flows in opposite directions on the two sides of the resonance, yielding a minimum metallicity (Scarano & Lépine 2013) and SFR (Mishurov et al. 2002). (ii) A decrease of the star-formation efficiency as proposed by Esteban et al. (2013). (iii) The accretion of pristine gas (Marino et al. 2012; Sánchez et al. 2014). (iv) The bar presence (e.g. Zaritsky et al. 1994; Martin & Roy 1994). The data in our sample only allow us to investigate the bar presence and the star formation rate along the galactic disks. Inspection in the GMOS-S r' acquisition images of AM1256B, AM1219A, AM2030A and AM2030B do not reveal the presence of any bar. Moreover, Sánchez et al.

(2014), investigated the effects of bars in the abundance gradients for the objects observed in the CALIFA survey. Sánchez et al. (2014) did not find differences in statistical terms between the slope of the abundance gradient for barred galaxies and the one for other objects. Therefore, we excluded the bar presence as the explanation for the flattening found in these four interacting galaxies of our sample.

To investigate if there is a minimum of SFR at the break region, we used the $H\alpha$ flux measured in our observation and the relation given by Kennicutt (1998)

$$\text{SFR}(M_{\odot}/\text{yr}) = 7.9 \times 10^{-42} L(H\alpha)(\text{erg/s}). \quad (3)$$

Since the absolute flux of $H\alpha$ was not obtained, our SFR values must be interpreted as a relative estimation and the present analysis is only useful to study the behavior of SFR along the AM 1256B, AM 1219A, AM 2030A and AM 2030B disks. In Fig. 13 the SFR versus R/R_{25} for the galaxies above are shown, the inner region where the steeper gradient was found is indicated. For two objects, AM 1219A and AM 2030B, we can see that the SFR minimum values are located very close to the regions where the oxygen gradient breaks, in agreement with Esteban et al. (2013). Only for the former we also found a minimum in the estimated metallicities indicating that this break zone could be associated with a corotation radius, as pointed out by Mishurov et al. (2002). For the other two objects, AM 1256B and AM 2030A, the breaks in the abundance gradients are located very close to the SFR maximum.

Another important issue is the behavior of the ionization parameter U with the metallicity. Basically, U represents the dimensionless ratio of the ionizing photon density to the electron density and it is defined as $U = Q_{ion}/4\pi R_{in}^2 n c$, where Q_{ion} is the number of hydrogen ionizing photons emitted per second by the ionizing source, R_{in} is the distance from the ionization source to the inner surface of the ionized gas cloud (in cm), n is the particle density (in cm^{-3}), and c is the speed of light. Therefore, due to the gas flow along the disk of interacting galaxies yield high values of electron density when compared to the ones found in isolated star-forming regions (Paper I), it is expected to find low U values in the H II regions located in our sample. To verify that, we used the spectroscopic data presented in Table 3 and the relation

$$\log U = -1.66 (\pm 0.06) \times S2 - 4.13 (\pm 0.07), \quad (4)$$

taken from Dors et al. (2011), where $S2 = \log([S II](\lambda 6717, \lambda 6731)/H\alpha)$. This equation is valid for $-1.5 \lesssim \log U \lesssim -3.5$ and estimations out of this range were not considered. These U estimations are plotted in Fig. 14 versus the O/H abundances determined from $N2$ for

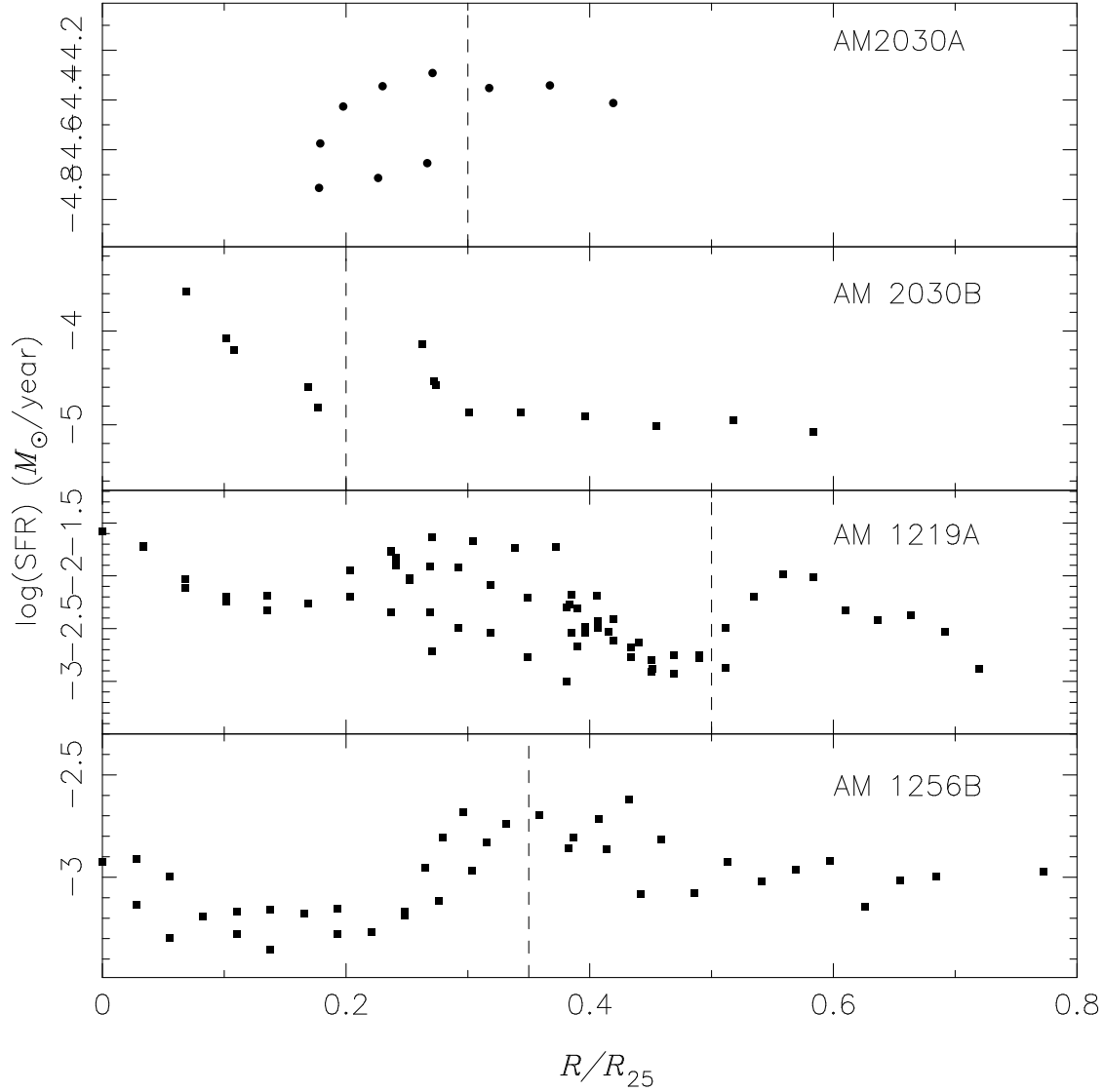


Figure 13. SFR vs. the galactocentric distance (R/R_{25}) for AM 1256B, AM 1219A, AM 2030B and AM 2030A. The dotted line separates the inner region where the steeper gradient was found (see text).

our sample, for H II regions in the interacting galaxy NGC 1512 observed by Bresolin et al. (2012) as well as estimations for star-forming regions in isolated galaxies obtained using the same calibrations and the data compiled by Dors et al. (2011). Also, the CALIFA data (Sánchez et al. 2012) for about 300 galaxies of any morphological type are included in this analysis. It can be seen that H II regions located in interacting galaxies do not present the lowest U values. However, there is a clear correlation indicating that the highest abundances are found in those regions of galaxies with lower ionization strength (see also Freitas-Lemes et al. 2013; Pérez-Montero 2014). In fact, H II regions located in the center of galaxies are more evolved (from their H α equivalent with) than the ones located in the outskirts regions, as pointed by Sánchez et al. (2012), having lower ionization strengths and higher, respectively.

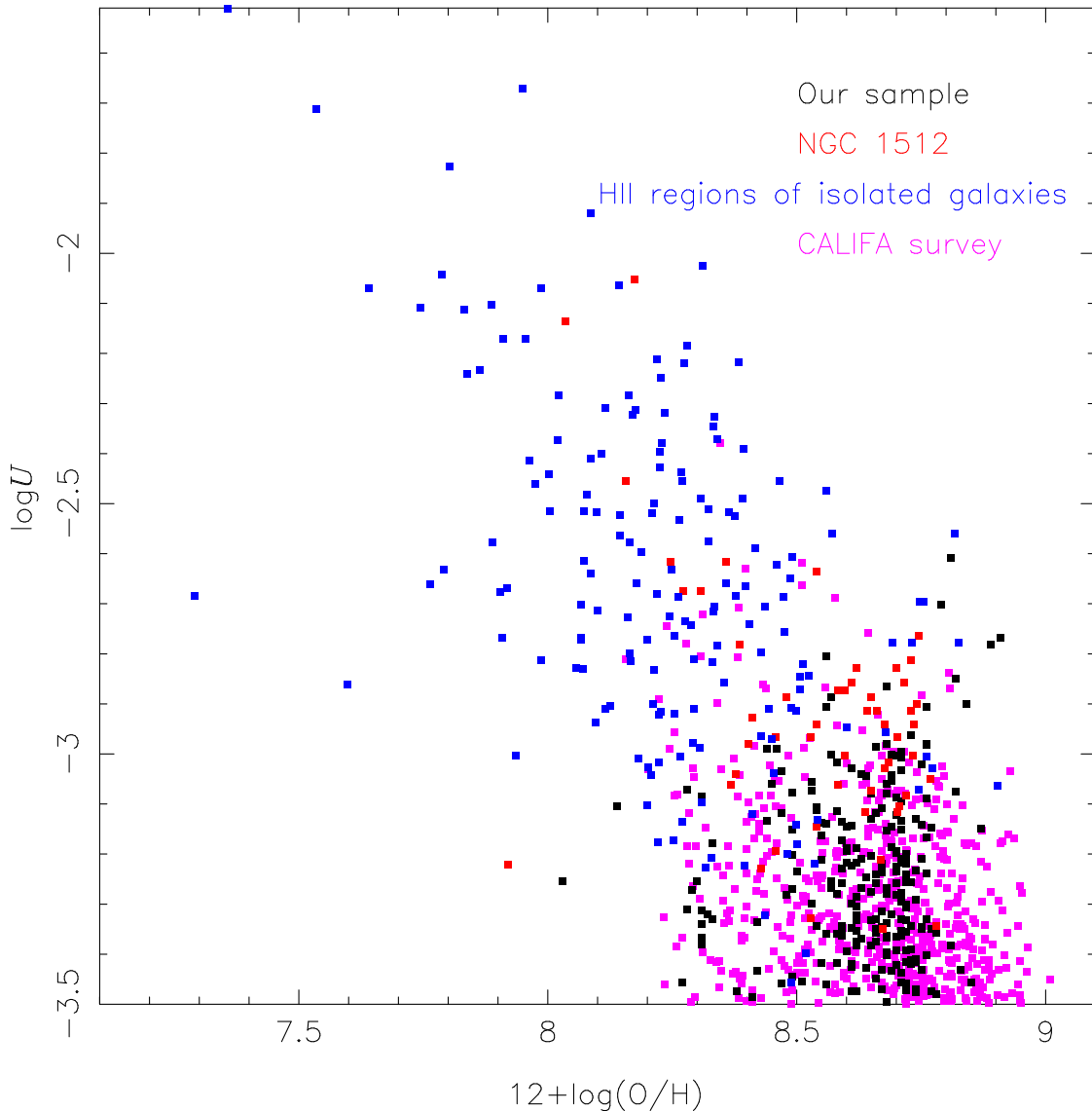


Figure 14. Ionization parameter U vs. the oxygen abundance of HII regions belonging to spiral galaxies from the CALIFA survey, isolated galaxies (data taken from Dors et al. 2011), NGC 1512 (Bresolin et al. 2012), and our sample as indicated. Estimations of O/H and U were obtained using Eqs. 1 and 4, respectively.

6 CONCLUSIONS

We presented an observational study about the oxygen gradient abundance in interacting galaxies. Long-slit spectra in the range 4400-7300 Å were obtained with the Gemini Multi-Object Spectrograph at Gemini South (GMOS) for eleven galaxies in eight close pairs. Spatial profiles of oxygen abundance (used as metallicity tracer) in the gaseous phase along galaxy disks were obtained using calibrations based on strong emission-lines ($N2$ and $O3N2$). We found oxygen gradients significantly flatter for all galaxies in the close pairs of our sample than the ones found in isolated spiral galaxies. For four objects of our sample, AM1219A, AM1256B, AM 2030A and AM2030B we found a clear break in the oxygen

abundance at galactocentric distances R/R_{25} of about 0.5, 0.35, 0.3, 0.2, respectively. For two objects, AM1219A and AM1256B, we found negative slopes for the inner gradients, and for AM2030B we found a positive one. In all these three cases they show a flatter behaviour to the outskirts of the galaxies. In the case of AM2030A, we found a positive-slope outer gradient while the inner one is almost compatible with a flat behaviour. This result is not concluding due to the small number of measured H II regions mainly for the outer part. We found a decrease of star formation efficiency in the zone that corresponds to the oxygen abundance gradient break for AM1219A and AM2030B. Moreover, in the case of AM1219A we also found a minimum in the estimated metallicities indicating that this break zone could be associated with a corotation radius. For the other two galaxies that present a gradient break, AM1256B and AM2030A, we found a maximum for the SFR but not an extreme oxygen abundance value. It must be noted that for all these four interacting systems the extreme SFR values are located very close to the oxygen gradient break zones. The flattening in the oxygen abundance gradients could be interpreted as being a chemical enrichment due to induced star formation by gas flows along the disks. We have found that H II regions located in close pairs of galaxies follow the same relation between the ionization parameter and the oxygen abundance as those regions in isolated galaxies.

ACKNOWLEDGEMENTS

Based on observations obtained at the Gemini Observatory, which is operated by the Association of Universities for Research in Astronomy, Inc., under a cooperative agreement with the NSF on behalf of the Gemini partnership: the National Science Foundation (United States), the Science and Technology Facilities Council (United Kingdom), the National Research Council (Canada), CONICYT (Chile), the Australian Research Council (Australia), Ministério da Ciencia e Tecnologia (Brazil), and SECYT (Argentina). D. A. Rosa, O. L. Dors Jr and A. C. Krabbe thanks the support of FAPESP, process 2011/08202-6, 2009/14787-7 and 2010/01490-3, respectively. We also thank to the anonymous referee for her/his careful and constructive revision of this manuscript.

REFERENCES

- Alonso-Herrero, A., Rosales-Ortega, F. F., Sánchez, S. F. et al. 2012, MNRAS, 425, L46
 Alloin, D., Collin-Souffrin, S., Joly, M., Vigroux, L., 1979, A&A, 78, 200

- Andrievsky, S. M., Kovtyukh, V. V., Luck, R. E. et al. 2002, *A&A*, 392, 491
- Andrievsky, S. M., Luck, R. E., Martin, P., Lépine, J. R. D. 2004, *A&A*, 413, 159
- Athanassoula, E. 1992, *MNRAS*, 259, 345
- Barden, M., Rix, H.-W., Somerville, R.S. et al. 2005, *ApJ*, 635, 959
- Barton, E. J., Geller, M. J., Kenyon, S. J. 2000, *ApJ*, 530, 660
- Bastian, N., Tranco, G., Konstantopoulos I. S., Miller, B. W., 2009, *ApJ*, 701, 607
- Bernloehr, K. 1993, *A&A*, 270, 20
- Bergvall, N., Laurikainen, E., Aalto, S. 2003, *A&A*, 405, 31
- Bragaglia, A., Sestito, P., Villanova, S. et al. 2008, *A&A*, 480, 79
- Bresolin, F., Kennicutt R. C., Ryan-Weber E., 2012, *ApJ*, 750, 122
- Bresolin, F. 2011, *ApJ*, 730, 129
- Bresolin, F., Gieren, W., Kudritzki, R. -P. et al. 2009, *ApJ*, 700, 309
- Bresolin, F., Schaerer, D., González Delgado, R. M., Stasińska, G. 2005, *A&A*, 441, 981
- Boissier, S., & Prantzos, N. 2000, *MNRAS*, 312, 398
- Bell, E. F., de Jong, R. S. 2000, *MNRAS*, 312, 497
- Bresolin, F., Ryan-Weber, E., Kennicutt, R. C., Goddard, Q. 2009, *ApJ*, 695, 580
- Cardelli J. A., Clayton, G. C., Mathis J. S., 1989, *ApJ*, 345, 245
- Castellanos, M., Díaz, A. I., Terlevich, E. 2002, *MNRAS*, 329, 315
- Chien, L., Barnes, J. E., Kewley, L. J., Chambers, K. C., 2007, *ApJ*, 660, L105.
- Cid Fernandes, R., Mateus, A., Sodré, L. et al. 2005, *MNRAS*, 358, 363
- Costa, R. D. D., Uchida, M. M. M., Maciel, W. J. 2004, *A&A*, 423, 199
- Dalcanton, J. J. 2007, *ApJ*, 658, 941
- Di Matteo, P., Bournaud, F., Martig, M. 2008, *A&A*, 492, 31
- Donzelli, C. J., Pastoriza, M. G., 1997, *ApJS*, 111, 181
- Dors, O. L., Krabbe, A. C., Hägele, G. F., Pérez-Montero, E. 2011, *MNRAS*, 415, 3616
- Dors, O. L., & Copetti, M. V. F. 2005, *A&A*, 437, 837
- Esteban, C., Carigi, L., Copetti, M. V. F. et al. 2013, *MNRAS*, 433, 382
- Ellison S. L., Mendel J. T., Patton D. R., Scudder J. M., 2013, *MNRAS*, 435, 3627
- Ferreiro, D. L., & Pastoriza, M. G. 2004, *A&A*, 428, 837
- Ferreiro, D. L., Pastoriza, M. G., Rickes, M., 2008, *A&A*, 481, 645
- Freedman Woods, D., Geller, M. J., Kurtz, M. J. et al. 2010, *AJ*, 139, 1857
- Freitas-Lemes, P., Rodrigues, I., Fáyndez-Abans, M., Dors, O. L., Fernandes, I. F. 2013, *MNRAS*, 427, 2772

- Friedli, D., Benz, W., Kennicutt, R. C. 1994, *ApJ*, 430, L105
- Garnett, D. R., Shields, G. A., Skillman, E. D., Sagan, S. P. , Dufour, R. J. 1997, *ApJ*, 489, 63.
- Goddard, Q. E., Bresolin F., Kennicutt R. C., Ryan-Weber, E. V., Rosales-Ortega, F. F. 2011, *MNRAS*, 412, 1246
- Hägele, G. F., Díaz, A. I., Terlevich E. et al. 2008, *MNRAS*, 383, 209
- ernandez-Jimenez, J. A., Pastoriza, M. G., Rodrigues, I. et al. 2013, *MNRAS*, 435, 3342
- Hummer, D. G., & Storey P. J. 1987, *MNRAS*, 224, 801
- Hernandez-Jimenez, J. A., Pastoriza, M. G., Rodrigues, I., Krabbe, A. C., Winge, C., Bonatto, C. 2013, *MNRAS*, 435, 3342
- López-Sánchez, A. R., & Esteban, C. 2010, *A&A*, 516, 104
- Luck, R. E., Gieren, W. P., Andrievsky, S. M. et al. 2003, 401, 939
- Lemasle, B., Franois, P., Genovali, K. et al. 2013, *A&A*, 558, 31
- Kennicutt, R. C., Bresolin, F., Garnett, D. R. 2003, *ApJ*, 591, 801
- Kennicutt, R. C. 1998, *ARAA*, 36, 189
- Kewley, L. J., Rupke, D., Zahid, H. J., Geller, M. J., Barton, E. J., 2010, *ApJ*, 721, L48
- Kewley, L. J., & Ellison, S. L., 2008, *ApJ*, 681, 1183
- Krabbe, A. C., Rosa, D. A., Dors, O. L. et al. 2014, *MNRAS*, 437, 1155
- Krabbe, A. C., Pastoriza, M. G., Winge, C. et al. 2011, *MNRAS*, 416, 38
- Krabbe, A. C., Pastoriza, M. G., Winge, C., Rodrigues, I., Ferreira, D. L. 2008, *MNRAS*, 389, 1593
- Maciel, W. J., & Costa, R. D. D. 2009, in *IAU Symposium*, Vol. 254, *IAU Symposium*, ed. J. Andersen, Nordströara, B. m, & J. Bland-Hawthorn, 38P
- MacArthur, L. A., Courteau, S., Bell, E., Holtzman, J. A. 2004, *ApJS*, 152, 175
- McGaugh, S. S. 1991, *ApJ*, 380, 140
- Magrini, L., Sestito, P., Randich, S., Galli, D. 2009, *A&A*, 494, 95
- Marino, R. A., Gil de Paz, A., Castillo-Morales, A. et al. 2012, *ApJ*, 754, 61
- Marino, R. A., Rosales-Ortega, F. F., Sánchez, S. F. et al. 2013, *A&A*, 559, 114
- Martin, P., & Roy, J. R. 1995, *ApJ*, 445, 161
- Martin, P., & Roy, J. R. 1994, *ApJ*, 424, 599
- Miralles-Caballero, D., Díaz, A. I., Rosales-Ortega, F. F., Pérez-Montero, E., Sánchez, S. F. 2014, *MNRAS*, 440, 2265
- Mihos, J. C., Bothun, G. D., Richstone, D. O. 2010, *ApJ*, 418, 82

- Mishurov, Y. N., Lépine, J. R. D., Acharova, I. A., 2002, ApJ, 571, L113
- Mólla, M., & Díaz, A. I. 2005, MNRAS, 358, 521
- Muñoz-Mateos, J. C., Gil de Paz, A., Boissier, S. et al. 2007, ApJ, 658, 1006
- Nikolic, B., Cullen, H., Alexander, P., 2004, MNRAS, 355, 874
- Lambas, D. G., Tissera, P. B., Alonso, M. S., Coldwell, G. 2003, MNRAS, 346, 1189
- Patton, D. R., Ellison, S. L., Simard, L. et al. 2011, MNRAS, 412, 591
- Paturel, G., Petit, C., Prugniel, P. et al. 2003, A&A, 412, 45
- Paturel, G., Garcia, A. M., Fouque, P., Buta, R. 1991, A&A, 243, 319
- Pedicelli, S., Bono, G., Lemasle, B. et al. 2009, A&A, 504, 81
- Pérez-Montero, E., & Contini, T., 2009, MNRAS, 398, 949
- Pérez-Montero, E. 2014, MNRAS, 441, 2663
- Pettini M., & Pagel B. E. J., 2004, MNRAS, 348, L59
- Pilyugin, L. S., Grebel, E. K., Mattsson, L. MNRAS, 424, 2316
- Pilyugin, L. S. 2003, A&A, 397, 109
- Pilyugin, L. S., & Thuan, T. X. 2005, ApJ, 631, 231
- Pohlen, M., & Trujillo, I. 2006, A&A, 454, 759
- Portinari, L., & Chiosi, C. 1999, A&A, 350, 827
- Rodríguez-Baras, M., Rosales-Ortega, F. F., Díaz, A. I., Sánchez, S. F., & Pasquali, A. 2014, MNRAS, 442, 495
- Rosales-Ortega, F. F., Díaz, A. I., Kennicutt, R. C., Sánchez, S. F. 2011, MNRAS, 415, 2439
- Rupke, D. S. N., Kewley, L. J., Barnes J. E. 2010a, ApJ, 710, L156
- Rupke, D. S. N., Kewley, L. J., Chien, L. -H. 2010b, ApJ, 723, 1255
- Scarano, S., & Lépine, J. R. D., 2013, MNRAS, 428, 625
- Scarano, S., Lépine, J. R. D., Marcon-Uchida, M. M., 2011, MNRAS, 412, 1741
- Sánchez, S. F., Rosales-Ortega, F. F., Marino, R. A. et al. 2012a, A&A, 546, 2
- Sánchez, S. F., Rosales-Ortega, F. F., Iglesias-Páramo, J. et al. 2014, A&A, 563, 49
- Scudder, J. M., Ellison, S. L., Torrey, P., Patton, D. R., Mendel, J. T., 2012, MNRAS, 426, 549
- Shaver, P. A., McGee, R. X., Newton, L. M., Danks, A. C., Pottasch, S. R. 1983, MNRAS, 204, 53
- Stasińska G., 2006, A&A, 454, L127
- Storchi-Bergmann T., Calzetti, D., Kinney, A. L. 1994, ApJ, 429, 572

- Toomre, A., & Toomre Juri 1972, ApJ, 178, 623
- Torres-Flores, S., Scarano, S., Mendes de Oliveira, C., de Mello, D. F., Amram, P., Plana, H., 2014, MNRAS, 438, 1894
- Trancho, G., Bastian, N., Miller, B. W., Schweizer, F. 2007, ApJ, 664, 284
- Trujillo, I., Rudnick, G., Rix, H.-W. et al. 2004, ApJ, 604, 521
- Vílchez, J. M., & Esteban, C. 1996, MNRAS, 280, 720
- Zahid, H. J., & Bresolin, F. 2011, AJ, 141, 192
- Zaritsky, D., Kennicutt, R. C., Huchra, J. P. 1994, ApJ, 420, 87
- Werk, J. K., Putman, M. E., Meurer, G. R., Santiago-Figueroa, N., 2011, ApJ, 735, 71
- Wright, E. L. 2006, PASP, 118, 1711
- Yong, D., Carney, B. W., Friel, E. D. 2014, AJ, 144, 95